ECCOMAS Congress 2016
VII European Congress on Computational Methods in Applied Sciences and Engineering
M. Papadrakakis, V. Papadopoulos, G. Stefanou, V. Plevris (eds.)
Crete Island, Greece, 5–10 June 2016

THE USE OF ENRICHED BASE FUNCTIONS IN THE THREE-DIMENSIONAL SCALED BOUNDARY FINITE ELEMENT METHOD

Sascha Hell[1] **and Wilfried Becker**[1]

[1]Institute of Structural Mechanics, Technical University of Darmstadt
Franziska-Braun-Straße 7, 64287 Darmstadt, Germany
e-mail: {hell,becker}@fsm.tu-darmstadt.de

Keywords: Scaled Boundary Finite Element Method, enriched base functions, three-dimensional linear elasticity, quadratic eigenvalue problem

Abstract. *The Scaled Boundary Finite Element Method (SBFEM) is a semi-analytical method which combines the advantages of the Boundary Element Method (BEM) and the Finite Element Method (FEM). Like in the BEM, only the boundary needs to be discretized. On the other hand, the SBFEM is based on the virtual work principle and does not need any fundamental solutions. If the scalability condition is fulfilled, a separation of variables representation can be employed leading to a quadratic eigenvalue problem and a linear equation system which can be solved by standard methods. The SBFEM has proven its high efficiency and accuracy in the presence of stress singularities, especially in 2D fracture mechanics when the singularity is entirely located within the considered domain.*

However, in 3D elasticity problems, there can also be singularities on the discretized boundary itself. Then, the SBFEM suffers from drawbacks also well known from the standard FEM, i.e. moderate accuracy and bad convergence. To overcome these deficiencies in such 3D cases, we propose the enrichment of the standard separation of variables representation with analytical fields which are known to exactly fulfill the local boundary conditions:

$$\boldsymbol{u} = \underbrace{\mathbf{N}(\eta_1, \eta_2)\, \boldsymbol{u}(\xi)}_{\text{standard}} + \underbrace{\mathbf{F}(r, \varphi)\, \boldsymbol{a}(\xi)}_{\text{enrichment}}. \tag{1}$$

The examples of a single plane crack and two perpendicularly meeting cracks in an isotropic continuum are considered. It is demonstrated that the method's original excellent accuracy and convergence are regained, at a minimum cost of additional degrees of freedom (DOF). The normalized errors in the solution of the quadratic eigenvalue problem already become negligibly small for very coarse boundary meshes. The obtained convergence orders are often optimal and sometimes even superconvergence is observed.

1 INTRODUCTION

This work is concerned with the efficient numerical solution of three-dimensional boundary value problems of linear elasticity which involve stress singularities. Stress singularities in linear elasticity theory involve infinite stresses and strains at certain points or lines which typically represent discontinuities of geometry (e.g. cracks and notches), material (e.g. multi-material junctions) or loading. Although such singularities cannot actually occur in a real material as they are locally reduced by non-linear deformations, in brittle materials, their near-field still is a good approximation to the real stress and displacement fields (e.g. already in 1927 their occurrence was considered by Knein [19] because he found his pressure test blocks to unexpectedly often fail at the corners instead of their center). Usually, as e.g. by Williams [38], the near-field solution at a singular point for the displacements and stresses respectively is represented by a power law function series of the kind

$$\underline{u}(r,\varphi,\vartheta) = \sum_{j=1}^{\infty} c_{uj} r^{\lambda_j} \underline{\phi}_{uj}(\varphi,\vartheta) \qquad , \qquad \underline{\underline{\sigma}}(r,\varphi,\vartheta) = \sum_{j=1}^{\infty} c_{\sigma j} r^{\lambda_j - 1} \underline{\underline{\phi}}_{\sigma j}(\varphi,\vartheta) \tag{2}$$

given in spherical coordinates r, φ, ϑ. Here, λ_j are complex exponents, $\underline{\phi}_{uj}$ are vector and $\underline{\underline{\Phi}}_{\sigma j}$ are tensor functions of the angle coordinates φ and ϑ. Line singularities can be similarly represented in e.g. cylindrical coordinates. The free constants c_{uj} respectively $c_{\sigma j}$ are determined by conformance to the boundary conditions.

It is considerably more difficult to find solutions for three-dimensional boundary value problems containing singularities than for two-dimensional ones. This resulted in the development and application of appropriate numerical (e.g. FEM [44]) but also semi-analytical methods (e.g. [6, 28, 4]). The probably most employed semi-analytical method for such elasticity problems is the FEM eigenanalysis, which has been used by a number of researchers for several 2D (e.g. [40, 42, 15, 30, 34, 43]) and 3D applications (e.g. [5, 32, 24, 13, 31, 9, 20, 26, 18]). The FEM eigenanalysis is based on the approximation of the displacements by a separation of variables representation with FE-shape functions in the circumferential direction, i.e. only the boundary needs to be discretized. This representation is substituted in the Galerkin method generally leading to a Cauchy-Euler differential equation system of second order. This, in turn, can be transformed into a quadratic eigenvalue problem. The solution of the quadratic eigenvalue problem yields approximations for the quantities λ_j and $\underline{\phi}_{uj}$ in eq. (2) but not for the free constants c_{uj}, which would be necessary to solve the complete boundary value problem. Generally, the solution of the complete quadratic eigenvalue problem is computationally expensive which practically was the main reason that the method was hardly used for the solution of complete boundary value problems.

The Scaled Boundary Finite Element Method (SBFEM) [34, 8, 39] is a variant of the FEM eigenanalysis technique. To the authors' knowledge, it was the first used to solve complete boundary value problems, but only for 2D situations. Its striking advantages in the treatment of 2D boundary value problems with stress singularities were consequently exploited (e.g. [33]) up to the development of codes which automatically predict crack growth ([41, 29, 7]). For 3D situations, it has lately been used e.g. by the current authors in [16].

A major challenge of the SBFEM in 3D situations containing singularities is that its accuracy and convergence properties suffer when line singularities reach the boundary mesh, meaning a loss of the method's initial advantages in the treatment of boundary value problems with singularities. Indeed, this is a phenomenon which also is well-known in the standard FEM (e.g. [35, 44]) and the usual remedy is a graded mesh with a strong refinement towards the

singularity. This approach has also been used for the FEM eigenanalysis (e.g. [2]) but still led to linearized eigenvalue problems so large that a complete solution with the QR-algorithm was avoided.

The QR-algorithm is computationally very expensive as its computational effort grows cubically with the number of degrees of freedom (DOF). But in return, it gives the complete set of eigenvalues and eigenvectors needed for the solution of the complete boundary value problem. Other solution methods for the quadratic eigenvalue problem, which have been implemented (e.g. [9]), are a lot more efficient but only partly solve the eigenvalue problem, i.e. they only give a small set of eigenpairs or only give the eigenvalues but not the eigenvectors. Thus, they can compensate the reduced convergence and accuracy with a strong refinement of the boundary mesh around the singularity but cannot be used to solve the complete boundary value problem. Consequently, an approach making it possible to still solve the complete eigenvalue problem while increasing the accuracy of the eigenpairs at a minimum cost of additional DOF is sought-after.

To the authors' knowledge, Lee and Im [23] have been the only ones engaged in this venture so far. They used simple quarter-point element formulations [17] to resolve a classical crack singularity on the boundary mesh. As this approach is limited to the classical crack singularity order, we propose a more general approach based on an enrichment of the separation of variables approach for the displacement field. In the past 20 years, such enrichment approaches have been intensely studied in the framework of the XFEM introduced by Belytschko and coworkers [10, 12]. From this stock of knowledge, we selected the DOF-efficient plateau method [22] in conjunction with blending element formulations [11, 37] and Fleming's decomposition of the crack tip near-field [10] for our implementation.

In section 2, the prerequisites of the newly developed method are presented. In section 3, its advantages regarding accuracy and convergence are demonstrated for the generic examples of a simple crack [1, 25] and two meeting cracks in a homogeneous isotropic cube [16]. Section 4 contains the major conclusions of our analyses.

2 THE SCALED BOUNDARY FINITE ELEMENT METHOD WITH ENRICHED DISPLACEMENT REPRESENTATIONS

Our three-dimensional SBFEM formulation (cf. [39], [16]) with an enriched displacement field is based on the virtual work principle

$$\delta W_i = \int_V \underline{\underline{\sigma}} : \delta\underline{\underline{\varepsilon}}\,\mathrm{d}V = \int_V \underline{f}^* \cdot \delta\underline{u}\,\mathrm{d}V + \int_{S_t} \underline{t}^* \cdot \delta\underline{u}\,\mathrm{d}A = \delta W_a \tag{3}$$

in which $\underline{\underline{\sigma}}, \delta\underline{\underline{\varepsilon}}, \underline{f}^*, \delta\underline{u}, \underline{t}^*$ are the stress tensor, the virtual strain tensor, body forces, virtual displacements and prescribed boundary tractions respectively. δW_i is the internal and δW_a the external virtual work. V is the volume of the considered domain and S_t the part of the domain's boundary with prescribed traction boundary conditions. We write stresses and strains in vector notation $\boldsymbol{\sigma}$ and $\boldsymbol{\varepsilon}$ and use a differential operator $\mathbf{L}$

$$\mathbf{L}^{\mathrm{T}} = \begin{bmatrix} \frac{\partial}{\partial x} & 0 & 0 & 0 & \frac{\partial}{\partial z} & \frac{\partial}{\partial y} \\ 0 & \frac{\partial}{\partial y} & 0 & \frac{\partial}{\partial z} & 0 & \frac{\partial}{\partial x} \\ 0 & 0 & \frac{\partial}{\partial z} & \frac{\partial}{\partial y} & \frac{\partial}{\partial x} & 0 \end{bmatrix} \tag{4}$$

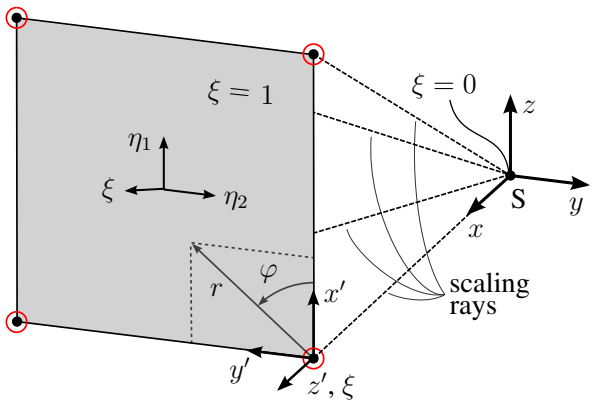

Figure 1: Plane, 4-node scaled boundary finite element forming a square-based pyramid (scaling center S with $\xi = 0$ at origin of a global cartesian coordinate system x, y, z). An isoparametric scaled boundary coordinate system ξ, η_1, η_2 and a conical coordinate system ξ, r, φ are present, the latter such that $r = 0$ at the crack front (singularity line) and $\varphi = \pm\pi$ at the crack faces. Enriched nodes are circled in red.

such that the equilibrium equations and strain-displacement relations can be written in matrix form

$$\sigma_{ij,j} + f_j = 0 \qquad \rightarrow \qquad \mathbf{L}^{\mathrm{T}}\boldsymbol{\sigma} + \boldsymbol{f} = \mathbf{0} \tag{5}$$

$$\varepsilon_{ij} = (u_{i,j} + u_{j,i})/2 \qquad \rightarrow \qquad \boldsymbol{\varepsilon} = \mathbf{L}\,\boldsymbol{u} \tag{6}$$

with $i, j = 1, 2, 3$. The latter relation is equally valid for the virtual displacements and strains. Furthermore, linear material behavior in the form of Hooke's law with the elasticity tensor in matrix notation $\mathbf{C}$ is assumed:

$$\boldsymbol{\sigma} = \mathbf{C}\,\boldsymbol{\varepsilon}. \tag{7}$$

The kinematic relations (6) and Hooke's law (7) are used in the virtual work principle (3) such that it can be given in terms of the displacements $\boldsymbol{u}$ and virtual displacements $\boldsymbol{\delta u}$:

$$\int_V \boldsymbol{\delta u}^{\mathrm{T}} \mathbf{L}^T \mathbf{C}\,\mathbf{L}\,\boldsymbol{u}\,\mathrm{d}V = \int_V \boldsymbol{\delta u}^{\mathrm{T}} \boldsymbol{f}\,\mathrm{d}V + \int_{S_t} \boldsymbol{\delta u}^{\mathrm{T}} \boldsymbol{t}^*\,\mathrm{d}A. \tag{8}$$

A fundamental prerequisite in the application of the SBFEM is that the considered elasticity problem is geometrically scalable, i.e. it must be possible to connect any point on a simply connected boundary to a chosen scaling center by a straight line (scaling ray), without this line meeting the boundary at any other point. An exception only is possible if the scaling center itself is located on the boundary and a scaling ray coincides with the boundary. In fact, this exceptional case is beneficially exploited in the analysis of cracks, V-notches and multimaterial corners. However, if the scalability condition is fulfilled, the displacement field can be expressed by a separation of variables representation. In the standard SBFEM for bounded domains (only one simply connected, outer boundary as it is exclusively considered within this work), the boundary is discretized creating pyramidal scaled boundary finite elements (SBFE). For each SBFE, an isoparametric formulation with a scaled boundary coordinate system is introduced (Fig. 1). The scaling coordinate ξ runs from the scaling center ($\xi = 0$) to the discretized boundary ($\xi = 1$). The boundary coordinates η_1, η_2 specify the position on the discretized boundary ($\eta_1, \eta_2 \in [-1, 1]$) each being zero at the center of the SBFE. This coordinate system is not necessarily orthonormal. Then, the approximated displacement field $\tilde{\boldsymbol{u}}_{st}^{(e)}$ of a standard SBFE e is represented as

$$\tilde{\boldsymbol{u}}_{st}^{(e)}(\xi, \eta_1, \eta_2) = \mathbf{N}(\eta_1, \eta_2)\,\boldsymbol{u}_n^{(e)}(\xi) \tag{9}$$

with 2D-element-shape-functions $\mathbf{N}(\eta_1, \eta_2)$ and nodal displacement functions $\boldsymbol{u}_n^{(e)}(\xi)$ on the scaling rays of the boundary nodes ($\xi \in [0, 1]$). Unless stated otherwise, the following derivations all apply to a single SBFE e. So from now on, the labeling $(\cdot)^{(e)}$ is omitted for brevity.

Our proposition is to enrich this separation of variables representation (9) by an additional field to better fulfill local boundary conditions at discontinuities, e.g. at crack faces:

$$\tilde{\boldsymbol{u}}(\xi, \eta_1, \eta_2) = \tilde{\boldsymbol{u}}_{st}(\xi, \eta_1, \eta_2) + \tilde{\boldsymbol{u}}_{enr}(\xi, \eta_1, \eta_2). \tag{10}$$

It is often advantageous to define a new conical coordinate system ξ, r, φ for this additional field. Its origin is placed at the scaling center as well and ξ again is the scaling coordinate. The scaled distance from the considered singularity line is denoted by r, while φ represents the angular coordinate. This coordinate system again is not necessarily orthonormal. Then, the separation of variables representation for the enriched field can be written in conical coordinates

$$\tilde{\boldsymbol{u}}_{enr}(\xi, r, \varphi) = \mathbf{F}(r, \varphi)\, \boldsymbol{a}(\xi). \tag{11}$$

with the enrichment functions $\mathbf{F}(r, \varphi)$ and their free coefficients $\boldsymbol{a}(\xi)$ which can be functions of the scaling coordinate. The coordinates r, φ can also be given in terms of the boundary coordinates η_1, η_2 if and only if the r, φ-plane and the η_1, η_2-plane are identical.

To be able to use the resulting enriched separation of variables representation in the virtual work principle (8), the differential operator $\mathbf{L}$ needs to be partitioned into the partial differential operators of the introduced coordinate systems.

$$\mathbf{L} = \mathbf{L}_x \frac{\partial}{\partial x} + \mathbf{L}_y \frac{\partial}{\partial y} + \mathbf{L}_z \frac{\partial}{\partial z} = \mathbf{L}_\xi \frac{\partial}{\partial \xi} + \mathbf{L}_{\eta_1} \frac{1}{\xi} \frac{\partial}{\partial \eta_1} + \mathbf{L}_{\eta_2} \frac{1}{\xi} \frac{\partial}{\partial \eta_2} = \mathbf{L}_\xi \frac{\partial}{\partial \xi} + \mathbf{L}_r \frac{1}{\xi} \frac{\partial}{\partial r} + \mathbf{L}_\varphi \frac{1}{\xi r} \frac{\partial}{\partial \varphi} \tag{12}$$

The partial differential operators $\mathbf{L}_x, \mathbf{L}_y, \mathbf{L}_z$ of the cartesian coordinate system and the corresponding Jacobi matrices $\mathbf{J}_\eta, \mathbf{J}_{r\varphi}$ are used to determine the partial differential operators $\mathbf{L}_\xi$, $\mathbf{L}_{\eta_1}$, $\mathbf{L}_{\eta_2}$, $\mathbf{L}_r$, $\mathbf{L}_\varphi$ of the conical and the scaled coordinate system. $\mathbf{L}_\xi$ happens to be identical for the conical and the scaled boundary coordinate system if the boundary is plane.

In the general case, the scaling center is located at certain coordinates $\boldsymbol{x_0}$ in a global cartesian coordinate system x, y, z. Then, the cartesian coordinates can be expressed in terms of the scaled boundary coordinates

$$\boldsymbol{x} = \boldsymbol{x_0} + \xi\, \boldsymbol{x_\eta}(\eta_1, \eta_2) \tag{13}$$

and in terms of the conical coordinates

$$\boldsymbol{x} = \boldsymbol{x_0} + \xi\, \boldsymbol{x_{r\varphi}}(r, \varphi) \tag{14}$$

where both $\boldsymbol{x_\eta}(\eta_1, \eta_2)$ and $\boldsymbol{x_{r\varphi}}(r, \varphi)$ denote the coordinates on the boundary ($\xi = 1$). These two equations describe the coordinate transformations needed for the determination of the Jacobi matrices. In this notation, the Jacobi matrices $\mathbf{J}_\eta(\eta_1, \eta_2)$ and $\mathbf{J}_{r\varphi}(r, \varphi)$ are functions of only the boundary coordinates so that the volumetric differential can be written as

$$\mathrm{d}V = \mathrm{d}x\, \mathrm{d}y\, \mathrm{d}z = \|\mathbf{J}_\eta(\eta_1, \eta_2)\|\, \xi^2\, \mathrm{d}\xi\, \mathrm{d}\eta_1\, \mathrm{d}\eta_2 = \|\mathbf{J}_{r\varphi}(r, \varphi)\|\, \xi^2 r\, \mathrm{d}\xi\, \mathrm{d}r\, \mathrm{d}\varphi. \tag{15}$$

Before the enriched displacement field approximation (10) is substituted in the virtual work principle (8), some terms of the differential operator and the enriched displacement field approximation should be combined. We distinguish between the standard SBFEM part of the displacement field approximation (9) and the enriching part (11). The shape functions $\mathbf{N}(\eta_1, \eta_2)$

in eq. (9) are combined with the partial differential operators of the scaled boundary coordinate system, resulting in the matrices $\mathbf{B}_\xi^{st}(\eta_1,\eta_2), \mathbf{B}_\eta^{st}(\eta_1,\eta_2)$.

$$\left[\mathbf{L}_\xi\frac{\partial}{\partial\xi}+\mathbf{L}_{\eta_1}\frac{1}{\xi}\frac{\partial}{\partial\eta_1}+\mathbf{L}_{\eta_2}\frac{1}{\xi}\frac{\partial}{\partial\eta_2}\right]\mathbf{N}(\eta_1,\eta_2)=\mathbf{B}_\xi^{st}(\eta_1,\eta_2)\frac{\partial}{\partial\xi}+\mathbf{B}_\eta^{st}(\eta_1,\eta_2)\frac{1}{\xi} \tag{16}$$

On the other hand, the enrichment functions $\mathbf{F}(r,\varphi)$ in eq. (11) are combined with the partial differential operators of the conical coordinate system, resulting in the matrices $\mathbf{B}_\xi^{enr}(r,\varphi)$ and $\mathbf{B}_{r\varphi}^{enr}(r,\varphi)$.

$$\left[\mathbf{L}_\xi\frac{\partial}{\partial\xi}+\mathbf{L}_r\frac{1}{\xi}\frac{\partial}{\partial r}+\mathbf{L}_\varphi\frac{1}{\xi r}\frac{\partial}{\partial\varphi}\right]\mathbf{F}(r,\varphi)=\mathbf{B}_\xi^{enr}(r,\varphi)\frac{\partial}{\partial\xi}+\mathbf{B}_{r\varphi}^{enr}(r,\varphi)\frac{1}{\xi} \tag{17}$$

Restructuring of the matrices leads to the following formulation of the product of the differential operator and the enriched displacement field approximation $\tilde{\boldsymbol{u}}$ (strain field approximation $\tilde{\boldsymbol{\varepsilon}}$, cf. eq. (6):

$$(\tilde{\boldsymbol{\varepsilon}}=)\ \mathbf{L}\,\tilde{\boldsymbol{u}}(\xi,\eta_1,\eta_2)=\left(\underbrace{\begin{bmatrix}\mathbf{B}_\xi^{st}\\ \mathbf{B}_\xi^{enr}\end{bmatrix}}_{\mathbf{B}_\xi(\eta_1,\eta_2)}\frac{\partial}{\partial\xi}+\underbrace{\begin{bmatrix}\mathbf{B}_\eta^{st}\\ \mathbf{B}_{r\varphi}^{enr}\end{bmatrix}}_{\mathbf{B}_\eta(\eta_1,\eta_2)}\frac{1}{\xi}\right)\underbrace{\begin{bmatrix}\boldsymbol{u}_n(\xi)\\ \boldsymbol{a}(\xi)\end{bmatrix}}_{\boldsymbol{u}_{nc}(\xi)} \tag{18}$$

with both coordinates r and φ being expressed in terms of η_1 and η_2. The vector $\boldsymbol{u}_{nc}$ contains the complete set of degrees of freedom on the boundary. Analogously, its virtual counterpart will be denoted $\boldsymbol{\delta u}_{nc}$. As it is assumed that this approximation also holds for the virtual displacements, the internal virtual work can be written as

$$\delta W_i=\int_V\left[\boldsymbol{\delta u}_{nc,\xi}^{\mathrm{T}}\,\mathbf{B}_\xi^{\mathrm{T}}+\boldsymbol{\delta u}_{nc}^{\mathrm{T}}\,\mathbf{B}_\eta^T\frac{1}{\xi}\right]\mathbf{C}\left[\mathbf{B}_\xi\,\boldsymbol{u}_{nc,\xi}+\mathbf{B}_\eta\,\boldsymbol{u}_{nc}\frac{1}{\xi}\right]\,\mathrm{d}V \tag{19}$$

This expression is identical to the standard SBFEM derivation except for the divergent formulation of the matrices $\mathbf{B}_\xi$ and $\mathbf{B}_\eta$. Expansion of the product and integration by parts over ξ results in an expression which can be integrated separately. Integration over the boundary coordinates η_1,η_2 yields the matrices

$$\begin{aligned}\mathbf{E}_0&=\int_{S_\xi}\mathbf{B}_\xi^{\mathrm{T}}(\eta_1,\eta_2)\,\mathbf{C}\,\mathbf{B}_\xi(\eta_1,\eta_2)\,\|\mathbf{J}_\eta(\eta_1,\eta_2)\|\,\mathrm{d}\eta_1\,\mathrm{d}\eta_2,\\ \mathbf{E}_1&=\int_{S_\xi}\mathbf{B}_\eta^{\mathrm{T}}(\eta_1,\eta_2)\,\mathbf{C}\,\mathbf{B}_\xi(\eta_1,\eta_2)\,\|\mathbf{J}_\eta(\eta_1,\eta_2)\|\,\mathrm{d}\eta_1\,\mathrm{d}\eta_2,\\ \mathbf{E}_2&=\int_{S_\xi}\mathbf{B}_\eta^{\mathrm{T}}(\eta_1,\eta_2)\,\mathbf{C}\,\mathbf{B}_\eta(\eta_1,\eta_2)\,\|\mathbf{J}_\eta(\eta_1,\eta_2)\|\,\mathrm{d}\eta_1\,\mathrm{d}\eta_2.\end{aligned} \tag{20}$$

S_ξ denotes the discretized boundary with constant scaling coordinate ξ. A numerical integration procedure is implemented but attention has to be paid that a sufficiently high integration order is used to account for the enrichment functions. In fact, we distinguish between integration of the purely standard SBFEM parts of the matrices, for which we can use appropriate low order Gauss integration schemes, and all other parts which also depend on the enrichment functions.

Nevertheless, we omitted special integration schemes otherwise used in literature (e.g. [22, 27, 37]) because we already achieved adequate accuracy with a simple high order Gauss integration. However, more sophisticated integration schemes surely would further improve the numerical efficiency.

If the considered boundary value problem involves more than one SBFE, which generally is the case, the element matrices $\mathbf{E}_0, \mathbf{E}_1, \mathbf{E}_2$ are similarly assemled like the element stiffness matrices in the standard Finite Element Method (FEM [44]). Then, they are substituted in the internal virtual work yielding one integral term and one boundary term which is to be evaluated at the boundaries $\xi = 0$ and $\xi = 1$.

$$\begin{aligned} - \quad & \int_0^1 \boldsymbol{\delta u}_{nc}^{\mathrm{T}}(\xi) \Big[\xi^2 \mathbf{E}_0 \boldsymbol{u}_{nc}(\xi)_{,\xi\xi} + \xi \Big[2\mathbf{E}_0 - \mathbf{E}_1 + \mathbf{E}_1^{\mathrm{T}} \Big] \boldsymbol{u}_{nc}(\xi)_{,\xi} + \Big[\mathbf{E}_1^T - \mathbf{E}_2 \Big] \boldsymbol{u}_{nc}(\xi) \Big] \, \mathrm{d}\xi \\ + \quad & \boldsymbol{\delta u}_{nc}^{\mathrm{T}}(\xi) \Big[\xi^2 \mathbf{E}_0 \boldsymbol{u}_{nc}(\xi)_{,\xi} + \xi \mathbf{E}_1^{\mathrm{T}} \boldsymbol{u}_{nc}(\xi) \Big]_{\xi=0}^{1} \quad = \quad \delta W_i \end{aligned} \tag{21}$$

If it is assumed that virtual external work terms are nonzero only at the discretized boundary S_ξ (i.e. stress free boundary conditions at all other boundaries), these terms are independent of the scaling coordinate so that they only interact with the boundary term of the internal virtual work. Then, the virtual work principle is fulfilled if the integrand of the integral term in the internal virtual work is zero on the one hand, which yields a homogeneous Cauchy-Euler differential equation system of second order. On the other hand, all remaining terms in the virtual work principle form a linear equation system for enforcing the boundary conditions at the discretized boundary S_ξ.

Cauchy-Euler differential equation systems can be solved using standard methods leading to a quadratic eigenvalue problem with eigenvalues λ and eigenvectors $\boldsymbol{\phi}$.

$$\Big(\lambda^2 \mathbf{E}_0 + \lambda \Big[\mathbf{E}_0 - \mathbf{E}_1 + \mathbf{E}_1^T \Big] + \Big[\mathbf{E}_1^T - \mathbf{E}_2 \Big] \Big) \, \boldsymbol{\phi} = \mathbf{0} \tag{22}$$

We solve the quadratic eigenvalue problem by, first, transforming it into a linear one at the cost of doubling the degrees of freedom, and second, applying the QR-algorithm implemented in the *eig()* function in the numerical mathematics software MATLAB.

If the solution does not contain any Jordan blocks, i.e. the geometric multiplicity of all the eigenvalues is equal to their algebraic one, the solution can be written as

$$\boldsymbol{u}_{nc}(\xi) = \boldsymbol{\Phi} \, \xi^{\boldsymbol{\lambda}} \, \boldsymbol{c} \tag{23}$$

with $\xi^{\boldsymbol{\lambda}}$ being a diagonal matrix with entries ξ^{λ_i} and $\boldsymbol{c}$ being a vector of free constants which are to be determined from the linear equation system for the boundary conditions at S_ξ. The matrix $\boldsymbol{\Phi}$ contains all eigenvectors $\boldsymbol{\phi}_i$, which in turn comprise the nodal boundary displacements and the enrichment functions' coefficients at the discretized boundary S_ξ.

Interpreting the eigenvectors $\boldsymbol{\phi}_i$ as deformation modes and the eigenvalues λ_i as their associated decay rates, this representation just matches the power series representation (2) for 3D boundary value problems containing singularities.

3 NUMERICAL RESULTS AND DISCUSSION

Next, we present some results that we obtained using this newly developed method. First, the situation of a simple crack in an isotropic homogeneous material is considered as a benchmark example before we proceed to the more complex structural situation of two meeting cracks as it has been studied in [16].

In both cases, a cubic domain containing the discontinuities is modeled as depicted in fig. 2. Only the boundary is discretized and plane 4- or 8-node SBFEs with linear or quadratic shape functions respectively are used. The scaling center is located at the cube's center and the cracks

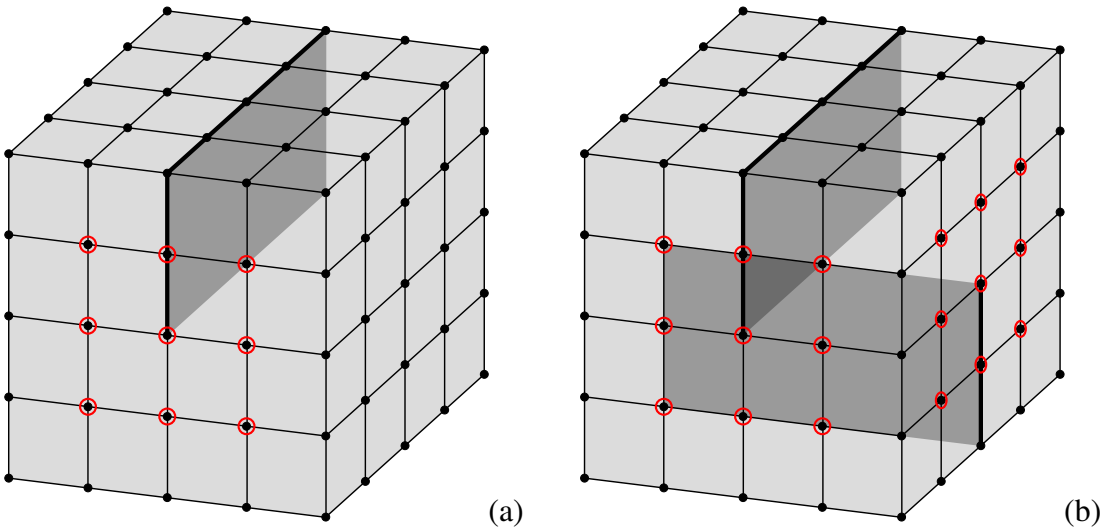

Figure 2: SBFE boundary meshes of cubes consisting of plane, 4-node SBFEs with (a) one crack (shaded) and (b) two meeting cracks. Enriched nodes are circled (red). Cracks are modeled using double nodes. The scaling center S is placed at the cube's center.

are modeled by inserting double nodes where a crack breaks the boundary. Consequently, the crack just reaches the scaling center and the crack front coincides with scaling rays. This also means that, contrary to the common practice in the popular XFEM which involves similar crack enrichments, the cracks are located between the elements instead of within them and there is no need for Heavyside enrichments.

The only enrichment functions needed are based on the classical crack tip near-field (e.g. [1, 14]). We adopt the decomposition of Fleming et al. [10]:

$$\mathbf{F}(r,\varphi) = \sqrt{r} \cdot [\sin(\varphi/2), \cos(\varphi/2), \sin(\varphi/2)\sin(\varphi), \cos(\varphi/2)\sin(\varphi)]. \tag{24}$$

Only nodes close to a crack front breaking through the boundary are enriched. For saving degrees of freedom (DOF) in the quadratic eigenvalue problem, which is essential for the numerical efficiency of its solution, the plateau method, e.g. used by [22, 11, 37], is adopted. In this method, all enriched nodes in the domain of influence of one crack tip are constrained to the same enrichment function coefficients, leading to only 4 additional DOF per dimension and per crack tip. In our formulation, it does not have to be accounted for crack tips but for locations where the crack front meets the boundary, leading to only $4 \cdot 3 \cdot 2 = 24$ additional DOF per crack.

As only certain domains and not all nodes are enriched, so-called blending elements are also needed. We follow the implementation of [11, 37] and denote the set of all nodes of one element $\mathcal{N}$ and the set only containing the element's enriched nodes $\mathcal{P}$. Furthermore, the values of the enrichment functions at the nodes are subtracted from the enrichment so that the functions $\boldsymbol{u}_n(\xi)$ remain the actual displacement functions at the scaling rays. Then, the complete separation of variables representation for the displacements in index notation can be written as

$$\begin{aligned}\tilde{u}_i(\xi,\eta_1,\eta_2) = &\sum_{k\in\mathcal{N}} N_k(\eta_1,\eta_2)\,\tilde{u}_{ik}(\xi) \quad + \\ &\sum_{l\in\mathcal{P}} N_l(\eta_1,\eta_2)\left[\sum_{m=1}^{n_F}\left(F_m(r,\varphi) - \sum_{k\in\mathcal{N}} N_k(\eta_1,\eta_2)\,F_m(r_k,\varphi_k)\right) a_{im}(\xi)\right]\end{aligned} \tag{25}$$

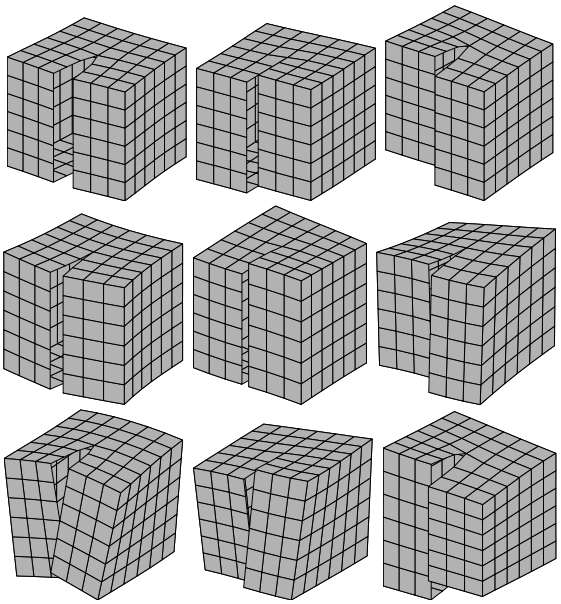

Figure 3: Deformation modes of a crack in an isotropic continuum for eigenvalues $\lambda = 0.5$ (1st line) and $\lambda = 1.5$. 1st line: classical crack modes I, II and III [1]. 2nd and 3rd line: modes IV, V, VI and VII,VIII,IX.

with $i = 1, 2, 3$ and n_F being the number of enrichment functions (here: $n_F = 4$). The coefficients of $\boldsymbol{u}_n(\xi)$ are simply denoted $\tilde{u}_{ik}(\xi)$. The quantities r_k and φ_k are the coordinates of the respective element nodes.

In fact, all elements on a cube face exhibiting a boundary breaking crack front contain enriched nodes and, consequently, require high order integration. Of course, the effect of the high integration order on the computational effort for the numerical integration is significant. For example, the computation time on a standard desktop PC (without exploiting any parallelization techniques), increases from 1.3 seconds (all elements with low order integration) to 9.3 seconds (high order integration at two cube faces) for a cube with 6 elements along each edge. But due to the increasing dominance of the computational effort necessary for solving the quadratic eigenvalue problem, the effect of the high integration order on the overall computational effort fades out with increasing mesh density.

The effect of the enrichment on the computational effort for solving the quadratic eigenvalue problem quickly becomes negligible as the number of elements n_e along each edge of a cube is increased because the enrichment for one crack only adds 24 DOFs while a standard SBFEM approach for a cube with one crack and $n_e = 6$ already results in $[(6n_e^2+2)+(2n_e-1)]\cdot 3 = 687$ DOF ($n_e = 10$: 1863 DOFs; $n_e = 20$: 7323 DOFs). On a standard desktop PC, the solution of the linearized quadratic eigenvalue problem using MATLAB's *eig()* function (QR-algorithm implementation) takes about 2.5 seconds for $n_e = 6$ but already about 42 seconds for $n_e = 10$ and 1655 seconds for $n_e = 20$. This, again, strongly emphasizes the need for a DOF-efficient formulation and implementation.

3.1 Crack in isotropic homogeneous continuum (benchmark example)

The benchmark example of an isotropic homogeneous continuum containing a single plane crack is considered (fig. 2a)) [1, 14]. In the three-dimensional solution, there are the three classical singular deformation modes with $\lambda = 0.5$ and six deformation modes with $\lambda = 1.5$. Please note, that three of the six deformation modes with decay rate $\lambda = 1.5$ cannot be found by a two-dimensional SBFEM analysis as they involve a displacement variation in the direction

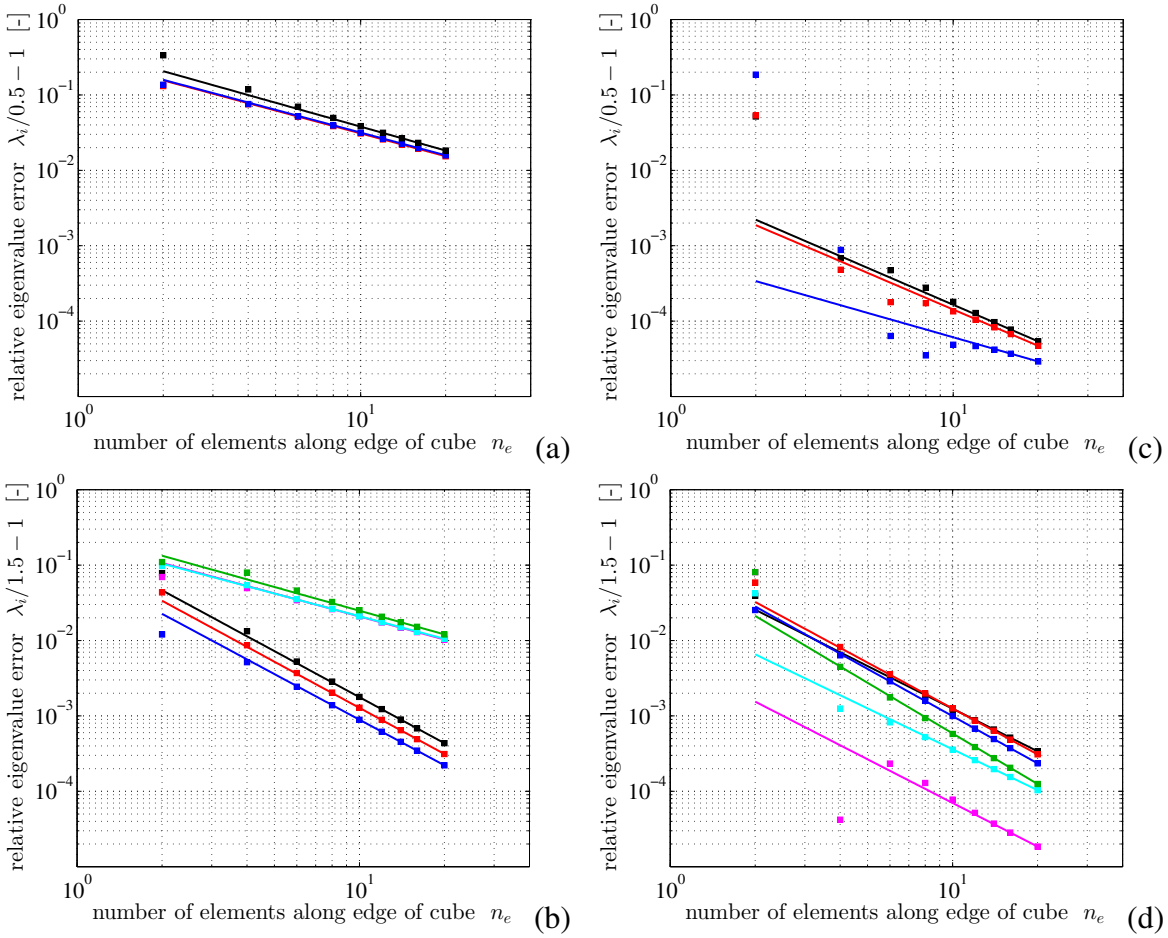

Figure 4: Convergence of some eigenvalues λ_i using the standard (a,b) and the enriched SBFEM (c,d), both with uniform meshing and linear 4-node SBFE (C4) (cf. fig. 2a). Plots (a,b) contain the classical crack modes I (red), II (blue) and III (black). Plots (c,d) contain the deformation modes IV (red), V (blue), VI (black), VII (magenta), VIII (cyan) and IX (green).

of the crack front (cf. fig. 3, 3[rd] line, deformation modes VII, VIII, IX).

In double logarithmic plots, fig. 4 shows the relative error of the calculated eigenvalues λ_i from the quadratic eigenvalue problem solution (22) to the analytical values of 0.5 and 1.5 for a uniform meshing with $n_e = 2, 4, 6, 8, 10, 12, 14, 16$ and 20 elements with linear shape functions (C4). As the computational effort quickly increases with an increasing number of DOF in the quadratic eigenvalue problem, computations with higher mesh densities were avoided. Yet at a glance, it can be seen that the enrichment of the displacement field leads to a tremendous reduction of the approximation error of the considered eigenvalues. Indeed, the relative error is reduced by several orders of magnitude, even for very low discretization levels: while the standard formulation with $n_e = 20$ elements along each edge of the cube and a computation time of about 30 minutes is not even capable of pushing the error in the singular modes below 1% (fig. 4a), the enriched formulation already attains an error $< 0.1\%$ for a discretization with only $n_e = 4$ and an overall computation time of 5 seconds (fig. 4c). It is to be noted that $n_e = 4$ actually is the lowest discretization which fully benefits from the enrichment because the discretization with $n_e = 2$ only contains blending and standard elements but no fully enriched ones.

The convergence orders mostly are considerably improved as well. However, at very low rel-

deformation mode	I	II	III	IV	V	VI	VII	VIII	IX
m_λ SBFEM (C4)	1.0	1.0	1.0	2.0	2.0	2.0	1.0	1.0	1.0
m_λ enrSBFEM (C4)	1.6	1.6	1.1	2.0	2.1	1.9	2.0	1.8	2.2

Table 1: Comparison of the approximated convergence orders m_λ of the standard (SBFEM) and the enriched formulation (enrSBFEM) with linear shape functions (C4) for considered deformation modes.

ative errors an improvement seems difficult, especially because the convergence is not always monotonic and only comparably low mesh densities were considered. Especially in the case of crack mode II (fig. 4c blue line and dots), we expect a further increase of the approximated convergence order with decreasing element size. Table 1 gives the approximated convergence orders m_λ of the eigenvalues λ_i. They were approximated from the last few values using a fitting procedure. The convergence orders achieved by the standard SBFEM formulation do not reach the optimal convergence order of $m_\lambda^{\text{opt}} = 2$ (e.g. [2]) for most of the considered deformation modes. For deformation modes I to III and VII to IX, we get the reduced convergence order of $m_\lambda \approx 1$ which indeed is the expected value when a singularity of order 0.5 is present on the mesh. Surprisingly, for the deformation modes IV, V and VI, which contrary to the deformation modes VII, VIII, IX also occur in a 2D SBFEM analysis, optimal convergence is achieved anyway but we do not have an explanation for this observation so far. However, the enriched formulation achieves about optimal convergence for all deformation modes IV to IX. For the deformation modes I to III, the convergence order is smaller but the relative error of the eigenvalues is of an almost negligible order of magnitude anyway.

Fig. 5 shows the relative error of the calculated eigenvalues λ_i from the quadratic eigenvalue problem solution (22) for a uniform meshing with $2, 4, 6, 8, 10$ and 12 elements n_e along the edge of the considered cube with quadratic shape functions (C8). A uniform mesh with $n_e = 12$ already accounts for $[(18n_e^2 + 2) + (4n_e - 1)] \cdot 3 = 7923$ DOF and a computation time of almost one hour for solving the complete eigenvalue problem. Thus, no finer meshes were considered, here. For SBFE with quadratic shape functions, an optimal convergence order of $m_\lambda^{\text{opt}} = 4$ is expected but not achieved for any eigenvalue or formulation considered. In the cases for which optimal convergence was achieved with linear shape functions (C4), now, the convergence order is bounded by the decay rate of the next two-dimensional deformation mode on the meshed plane which cannot be resolved by a polynomial. This is the decay rate and eigenvalue $\lambda = 1.5$ resulting in a maximum convergence order of $m_\lambda = 3$ as long as this deformation mode is not included in the enrichment. Nevertheless, wherever this increased convergence rate is achieved, there also is a considerable gain in accuracy. Otherwise, the error reduction may seem rather small when discretizations with the same number of nodes along each edge of the cube are compared. But there is an additional gain in efficiency as the employed serendipity elements (C8) have only 8 nodes instead of 9 and, thus, less DOF than a comparable mesh with 4-node elements. Finally, it should be mentioned that, naturally, the approximation of eigenvalues $\lambda = 2$ is distinctly superior compared to SBFE with linear shape functions (C4). Consequently, 8-node SBFE (C8) seem preferable whenever they are applicable.

Up to this point, only the error of the eigenvalues λ_i has been studied. We would like to complete this section with a consideration of the quality of the eigenvectors $\boldsymbol{\phi}_i$, i.e. the actual deformation modes (angular functions in eq. (2)). Here, we concentrate on the classical crack modes, which pertain to the eigenvalue $\lambda = 0.5$. The first check involves the coefficients $a_{im}(\xi)$ of the enrichment functions $F_m(r, \varphi)$ (eq. 24). To be able to exactly reproduce the analytical displacement fields [25, 14] given below, they must fulfill certain relations which we are going

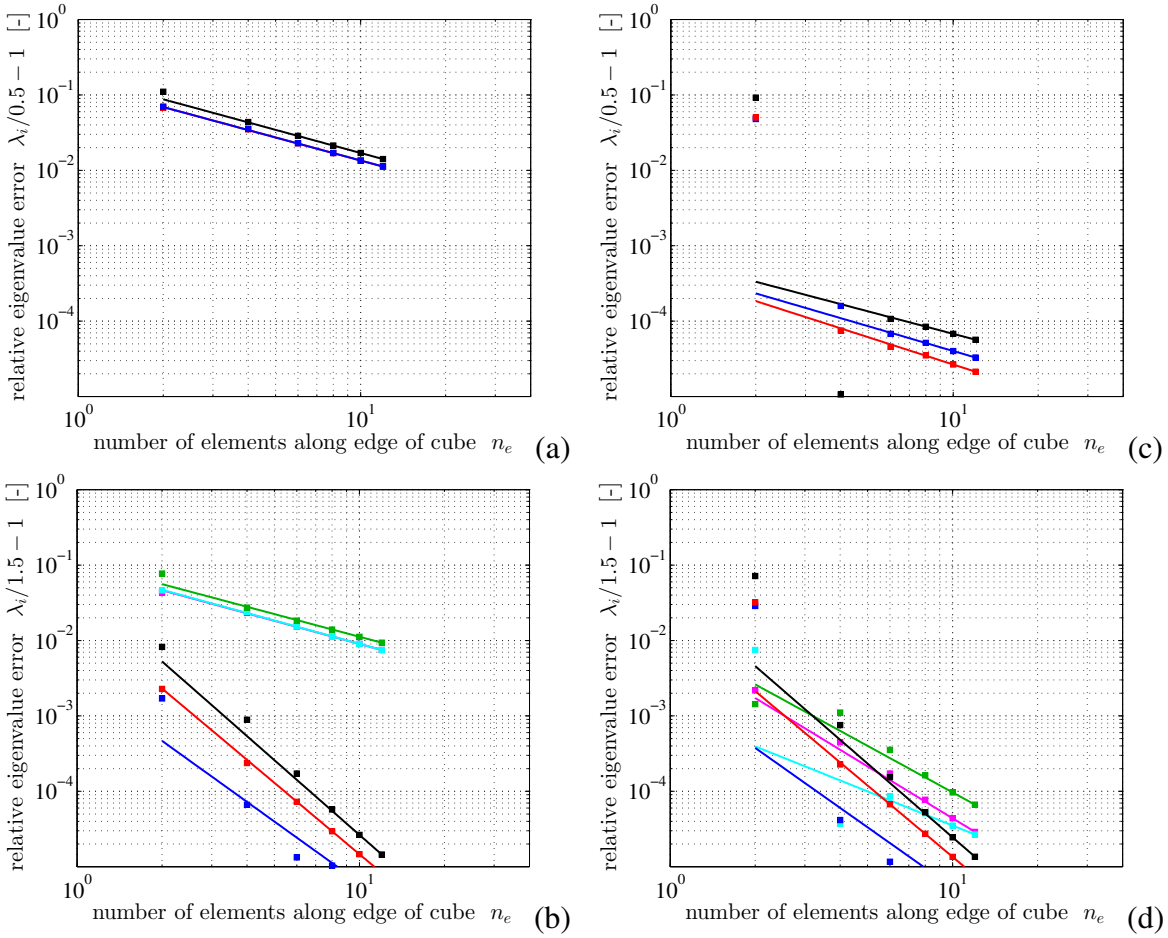

Figure 5: Convergence of some eigenvalues λ_i using the standard (a,b) and the enriched SBFEM (c,d), both with uniform meshing and quadratic 8-node serendipity elements (C8). Plots (a,b) contain the classical crack modes I (red), II (blue) and III (black). Plots (c,d) contain the deformation modes IV (red), V (blue), VI (black), VII (magenta), VIII (cyan) and IX (green).

to examine in the following (cf. Table 2 column 2).

$$\underline{u}_I(r,\varphi) = \frac{K_I}{2G}\sqrt{\frac{r}{2\pi}}(\kappa - \cos(\varphi)) \begin{bmatrix} \cos(\varphi/2) \\ \sin(\varphi/2) \\ 0 \end{bmatrix} \qquad \text{mode I} \tag{26}$$

$$\underline{u}_{II}(r,\varphi) = \frac{K_{II}}{2G}\sqrt{\frac{r}{2\pi}} \begin{bmatrix} \sin(\varphi/2)[2+\kappa+\cos(\varphi)] \\ \cos(\varphi/2)[2-\kappa-\cos(\varphi)] \\ 0 \end{bmatrix} \qquad \text{mode II} \tag{27}$$

$$\underline{u}_{III}(r,\varphi) = \frac{2K_{III}}{G}\sqrt{\frac{r}{2\pi}} \begin{bmatrix} 0 \\ 0 \\ \sin(\varphi/2) \end{bmatrix} \qquad \text{mode III} \tag{28}$$

The shear modulus is denoted by G and Poisson's ratio by ν. Further, it is $\kappa = 3 - 4\nu$ for plane strain assumptions, which, different from plane stress assumptions, make use of the full elasticity tensor and are completely consistent with the governing equations of 3D linear elasticity.

For a simpler comparison, we use the following enrichment functions for our reference cal-

	required relations	analytical	enrSBFEM (8x8C4)	relative deviation
crack mode I	$a_{12}/a_{14} = -\kappa$	-1.8	-1.800213	+0.012%
	$a_{21}/a_{23} = -\kappa$	-1.8	-1.799897	-0.006%
crack mode II	$a_{11}/a_{13} = \kappa + 2$	+3.8	+3.802018	+0.053%
	$a_{22}/a_{24} = \kappa - 2$	-0.2	-0.202246	+1.123%

Table 2: Comparison of analytical and numerical coefficient relations for crack modes I and II.

culation with $n_e = 8$ and linear shape functions (C4):

$$\mathbf{F}(r, \varphi) = \sqrt{r} \cdot [\sin(\varphi/2), \cos(\varphi/2), \sin(\varphi/2)\cos(\varphi), \cos(\varphi/2)\cos(\varphi)]. \tag{29}$$

They are more convenient because they better conform to the analytical field (26-28) but are still equivalent to Fleming's approach [22]. Table 2 shows the analytical coefficient relations and the results obained numerically for a material with a Poisson's ratio $\nu = 0.3$. It can be seen that the relative deviation of the numerically obtained values from the analytical ones for crack modes I and II is rather small. A further requirement for the exact representation of the analytical fields of crack modes I and II is that all other coefficients should be zero. Indeed, most of them are numerically zero and only single coefficients reach values of maximum 0.1% (mode I) and 0.03% (mode II) of the largest coefficient pertaining to the respective crack mode. Crack mode III only contains one analytical coefficient a_{31} which is none-zero, so the only requirement resulting from this crack mode is that all other coefficients are zero, which also is fulfilled (maximum relative deviation 0.006%).

After the comparison of the enrichment contribution of the displacement approximation, which naturally is only valid within the enriched pyramidal parts of the cube, now, the behavior along the crack front is considered. The left plot in Fig. 6 shows the variation of the magnitude of the displacements of each crack mode along a path running parallel to the crack front at a distance of 1/6 (dashed lines) and 1/3 (solid lines) of the considered cube's edge length. The figure for the example of $n_e = 6$ elements along a cube's edge with linear shape functions (C4) is symmetric as it is to be expected. It can be seen that the variation of the magnitude of displacements is marginal. The right plot showing the relative displacement magnitude with respect to the boundary values confirms this observation as the relative deviation remains $< 0.7\%$. The contribution of the enrichments to the displacement magnitude is neglected. This results in a piecewise linear form whose first (solid lines) respective second (dashed lines) section corresponds to a blending element where the largest part of the deviation initiates.

The actual magnitude of the displacements is of minor interest as the deformation modes' scaling indeed is arbitrary and only affects the stress intensity factors in a complete boundary value problem which we here do not intend to solve. Under the obvious assumption that the analytical fields are best matched within the enriched elements, it is most important, how the displacements inside the cube deviate from those at the enriched cube faces. From the obtained results for the rather coarse mesh, we conclude this deviation to be of negligible magnitude.

3.2 Two meeting cracks in homogeneous isotropic continuum

In this section, the more complex structural situation of two plane, perpendicularly meeting cracks (fig. 2b) studied in [16] is revisited and the convergence behavior of the first six eigenvalues resulting in stress singularities is investigated. The associated deformation modes are depicted and labeled in figure 7.

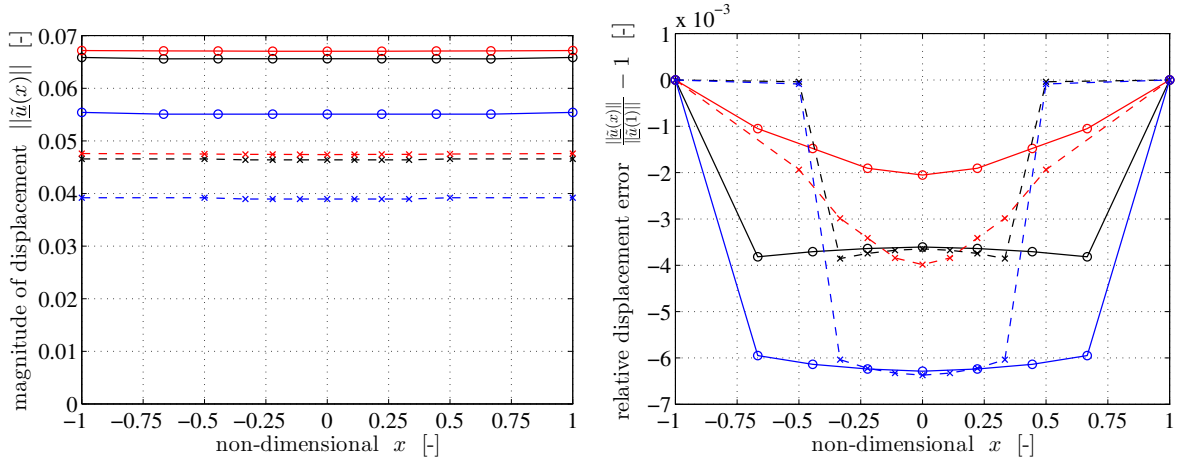

Figure 6: Plot of magnitude of displacements (left) and relative deviation of the displacement magnitude with respect to the boundary displacements (right) over a non-dimensional coordinate parallel to the crack front for crack modes I (red), II (blue), III (black). They are given on one crack face at 1/3 (dashed lines) and 2/3 (solid lines) of the distance of the crack front to the outer boundary for the example of $n_e = 6$ (C4). The displacement contribution of the enrichments is neglected.

As no analytical and, accordingly, no exact reference solution is known for this situation, the converged values are identified by a Richardson extrapolation, i.e. a function of the type $\lambda = C\, n_e^{m_\lambda} \lambda^{ext}$ is fitted to the numerical data. The quantities n_e (number of elements along edge of cube) and m_λ (convergence order) have already been introduced in the previous section. The eigenvalue approximated by the numerical procedure is denoted as λ. λ^{ext} is the extrapolated "exact" eigenvalue and C is a free constant.

deformation mode	*co1*	*co2*	*cs1*	*cs2*	*ct1*	*ct2*
λ^{ext} SBFEM	0.38260	0.67315	0.50749	0.50749	0.33982	0.79260
λ^{ext} enrSBFEM	0.38241	0.67299	0.50775	0.50775	0.33846	0.79206
m_λ SBFEM (C4)	1.0	1.2	1.0	1.0	1.2	1.0
m_λ enrSBFEM (C4)	1.8	1.8	1.5	1.5	2.9	2.0

Table 3: Comparison of the identified convergence orders m_λ of the standard (SBFEM) and the enriched formulation (enrSBFEM) with linear shape functions (C4) for the considered deformation modes.

Table 3 shows the results from this extrapolation procedure for the standard SBFEM formulation and the enriched one. It can be seen that the extrapolated eigenvalues λ^{ext} in essence coincide for both methods, but also that the associated orders of convergence differ considerably. While the convergence order of the standard formulation hardly exceeds the value of $m_\lambda = 1$, this value is easily surpassed by the enriched formulation. The eigenvalue associated to deformation mode *ct1* converges considerably faster than the others. In fact, even superconvergence seems to be achieved for this deformation mode but, up to date, we lack an explanation for this phenomenon.

From fig. 8, it can furthermore be concluded that the relative error in the eigenvalues is reduced by approximately two orders of magnitude when the enriched formulation is employed.

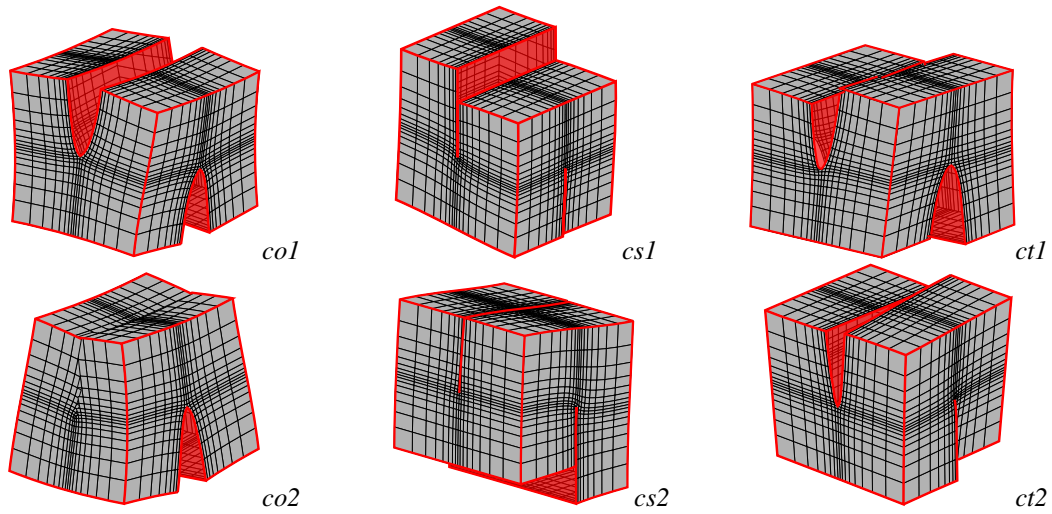

Figure 7: Deformation modes of two plane, perpendicularly meeting cracks in a homogeneous isotropic continuum for a cubical boundary mesh: 2 crack opening modes (*co1/2*), 2 crack shearing modes (*cs1/2*), 2 crack twisting modes (*ct1/2*).

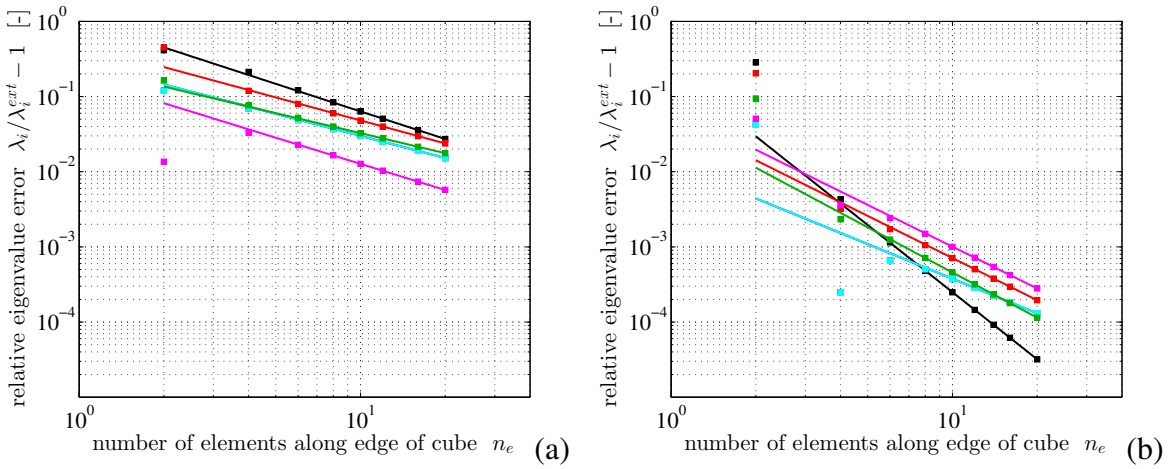

Figure 8: Convergence of first six eigenvalues λ_i which result in stress singularities using the standard (a) and the enriched SBFEM (b), both with uniform meshing and linear 4-node SBFE (C4). The corresponding deformation modes are *co1* (red line), *co2* (magenta), *cs1* (blue), *cs2* (cyan), *ct1* (black) and *ct2* (green).

4 SUMMARY AND CONCLUSIONS

It was our goal to improve the efficiency of the solution of three-dimensional linear elastic boundary value problems containing stress singularities. In the semi-analytical FEM eigenanalysis techniques like the SBFEM, a separation of variables representation can be employed in the virtual work principle if the scalability requirement is fulfilled. This leads to a differential equation system (DES) of second order which can be transformed into a quadratic eigenvalue problem. The obtained solution of the DES is of power series form. Additionally, a linear equation system (LES) for the conformance of the DES solution to the boundary conditions is obtained. Only the boundary needs to be discretized, typically using linear shape functions similar to those in the standard FEM. This results in a considerable reduction of the degrees of freedom so that the low computational efficiency of the eigenvalue solvers often only has a negligible effect on the overall efficiency of the method. Consequently, the SBFEM has already proven its suitability in the two-dimensional case.

However, in the three-dimensional case, we have demonstrated its deficiencies when a stress singularity is present on the discretized boundary. Then, the relative error increases by orders of magnitude and the convergence order is reduced by a factor of 2. As a similar phenomenon is also known from standard FEM techniques, the employment of their remedies seems natural.

We selected the enrichment approach to be the most suitable one and implemented a separation of variables representation enriched with the classical crack's near-field. For the example of a single plane crack in an isotropic continuum, we demonstrated that, at the cost of only 24 additional degrees of freedom, excellent accuracy of both the eigenvalues and eigenvectors can already be achieved for a very coarse boundary mesh. Moreover, due to the implemented plateau method, this number of additional degrees of freedom is independent of other meshing parameters. It only depends on the number of enrichment functions and the number of singular points on the boundary mesh. The obtained convergence order also is substantially improved, often optimal and sometimes even superconvergence is observed.

For the more complex example of two plane cracks meeting perpendicularly in a homogeneous isotropic continuum, the results could not be compared to an analytic reference solution. So, the converged eigenvalues were estimated using a Richardson extrapolation and the relative error was computed with respect to these values. Indeed, the standard SBFEM and the enriched formulation yielded almost the same extrapolated eigenvalues, but with a very different relative accuracy and convergence order.

We conclude that the proposed approach, which can easily be coupled with standard 3D finite elements, has turned out to be uniquely DOF-efficient. In our opinion, it thus shows the potential of providing easy access to the general solution of complete 3D linear elastic boundary value problems containing stress singularities (instead of only determining singularity order and possibly also mode). Although, its excellent accuracy and convergence properties have so far only been shown for the classical crack singularity, we hope to extend its applicability to more general cases (notch singularities, multi-material junctions, etc.) in future works.

REFERENCES

[1] T. L. Anderson and T. L. Anderson. *Fracture mechanics: fundamentals and applications*. CRC press, 2005.

[2] T. Apel, A.-M. Sändig, and S. I. Solov'ev. Computation of 3D vertex singularities for linear elasticity: Error estimates for a finite element method on graded meshes. *ESAIM: Mathematical Modelling and Numerical Analysis*, 36:1043–1070, 11 2002.

[3] S. N. Atluri, A. S. Kobayashi, and M. Nakagaki. An assumed displacement hybrid finite element model for linear fracture mechanics. *International Journal of Fracture*, 11(2):257–271, 1975.

[4] R. S. Barsoum. Theoretical basis of the finite element iterative method for the eigenvalue problem in stationary cracks. *International Journal for Numerical Methods in Engineering*, 26(3):531–539, 1988.

[5] Z. P. Bažant and L. F. Estenssoro. Surface singularity and crack propagation. *International Journal of Solids and Structures*, 15(5):405–426, 1979.

[6] J. P. Benthem. State of stress at the vertex of a quarter-infinite crack in a half-space. *International Journal of Solids and Structures*, 13(5):479–492, 1977.

[7] S. Dai, C. Augarde, C. Du, and D. Chen. A fully automatic polygon scaled boundary finite element method for modelling crack propagation. *Engineering Fracture Mechanics*, 133:163–178, 2015.

[8] A. J. Deeks and J. P. Wolf. A virtual work derivation of the scaled boundary finite-element method for elastostatics. *Computational Mechanics*, 28(6):489–504, 2002.

[9] A. Dimitrov, H. Andrä, and E. Schnack. Efficient computation of order and mode of corner singularities in 3D-elasticity. *International Journal for Numerical Methods in Engineering*, 52(8):805–827, 2001.

[10] M. Fleming, Y. A. Chu, B. Moran, T. Belytschko, Y. Y. Lu, and L. Gu. Enriched element-free Galerkin methods for crack tip fields. *International Journal for Numerical Methods in Engineering*, 40(8):1483–1504, 1997.

[11] T.-P. Fries. A corrected XFEM approximation without problems in blending elements. *International Journal for Numerical Methods in Engineering*, 75(5):503–532, 2008.

[12] T.-P. Fries and T. Belytschko. The extended/generalized finite element method: An overview of the method and its applications. *International Journal for Numerical Methods in Engineering*, 84(3):253–304, 2010.

[13] F. Ghahremani. A numerical variational method for extracting 3D singularities. *International Journal of Solids and Structures*, 27(11):1371–1386, 1991.

[14] D. Gross and T. Seelig. *Bruchmechanik: Mit einer Einführung in die Mikromechanik*. Springer Berlin Heidelberg, 2011.

[15] L. Gu and T. Belytschko. A numerical study of stress singularities in a two-material wedge. *International Journal of Solids and Structures*, 31(6):865–889, 1994.

[16] S. Hell and W. Becker. The scaled boundary finite element method for the analysis of 3D crack interaction. *Journal of Computational Science*, 9:76–81, 2015. Computational Science at the Gates of Nature.

[17] R. D. Henshell and K. G. Shaw. Crack tip finite elements are unnecessary. *International Journal for Numerical Methods in Engineering*, 9(3):495–507, 1975.

[18] N. Khaji and M. I. Khodakarami. A semi-analytical method with a system of decoupled ordinary differential equations for three-dimensional elastostatic problems. *International Journal of Solids and Structures*, 49(18):2528–2546, 2012.

[19] M. Knein. *Zur Theorie des Druckversuchs*, volume 7 of *Abhandlungen aus dem Aerodynamischen Institut an der Technischen Hochschule Aachen*, pages 43–62. Springer Berlin Heidelberg, 1927.

[20] H. Koguchi and T. Muramoto. The order of stress singularity near the vertex in three-dimensional joints. *International Journal of Solids and Structures*, 37(35):4737–4762, 2000.

[21] M. Kuna. *Numerische Beanspruchungsanalyse von Rissen: Finite Elemente in der Bruchmechanik*. Vieweg+Teubner, Wiesbaden, 2008.

[22] P. Laborde, J. Pommier, Y. Renard, and M. Salaün. High order extended finite element method for cracked domains. *International Journal for Numerical Methods in Engineering*, vol. 64(n? 3):pp. 354–381, September 2005.

[23] Y. Lee and S. Im. On the computation of the near-tip stress intensities for three-dimensional wedges via two-state M-integral. *Journal of the Mechanics and Physics of Solids*, 51(5):825–850, 2003.

[24] D. Leguillon and E. Sanchez-Palencia. *Computation of singular solutions in elliptic problems and elasticity*. John Wiley & Sons, Inc., 1987.

[25] J. Lemaitre and J.-L. Chaboche. *Mechanics of solid materials*. Cambridge University Press, 1994.

[26] C. Mittelstedt and W. Becker. Efficient computation of order and mode of three-dimensional stress singularities in linear elasticity by the boundary finite element method. *International Journal of Solids and Structures*, 43(10):2868–2903, 2006.

[27] S. Mohammadi. *XFEM fracture analyses of composites*. John Wiley & Sons, Ltd, 2012.

[28] N. V. Movchan and J. R. Willis. Surface-breaking crack in an elastic half-space. *Journal of Engineering Mathematics*, 37(1-3):143–154, 2000.

[29] E. T. Ooi, H. Man, S. Natarajan, and C. Song. Adaptation of quadtree meshes in the scaled boundary finite element method for crack propagation modelling. *Engineering Fracture Mechanics*, 144:101–117, 2015.

[30] S. S. Pageau and S. B. Biggers. A finite element approach to three-dimensional singular stress states in anisotropic multi-material wedges and junctions. *International Journal of Solids and Structures*, 33(1):33–47, 1996.

[31] C. R. Picu and V. Gupta. Three-dimensional stress singularities at the tip of a grain triple junction line intersecting the free surface. *Journal of the Mechanics and Physics of Solids*, 45(9):1495–1520, 1997.

[32] N. Somaratna and T. C. T. Ting. Three-dimensional stress singularities in anisotropic materials and composites. *International Journal of Engineering Science*, 24(7):1115–1134, 1986.

[33] C. Song. Analysis of singular stress fields at multi-material corners under thermal loading. *International Journal for Numerical Methods in Engineering*, 65(5):620–652, 2006.

[34] C. Song and J. P. Wolf. The scaled boundary finite-element method—alias consistent infinitesimal finite-element cell method—for elastodynamics. *Computer Methods in Applied Mechanics and Engineering*, 147(3–4):329–355, 1997.

[35] P. Tong and T. H. H. Pian. On the convergence of the finite element method for problems with singularity. *International Journal of Solids and Structures*, 9(3):313–321, 1973.

[36] P. Tong, T. H. H. Pian, and S. J. Lasry. A hybrid-element approach to crack problems in plane elasticity. *International Journal for Numerical Methods in Engineering*, 7(3):297–308, 1973.

[37] G. Ventura, R. Gracie, and T. Belytschko. Fast integration and weight function blending in the extended finite element method. *International Journal for Numerical Methods in Engineering*, 77(1):1–29, 2009.

[38] M. L. Williams. Stress Singularities Resulting From Various Boundary Conditions. *Journal of Applied Mechanics*, 19(4):526–528, 1952.

[39] J. P. Wolf. *The scaled boundary finite element method*. John Wiley & Sons, 2003.

[40] Y. Yamada and I. Nishiguchi. Concept of general parametric elements and applications. *Computers & Structures*, 19(1–2):277–284, 1984. Special Memorial Issue.

[41] Z. Yang. Fully automatic modelling of mixed-mode crack propagation using scaled boundary finite element method. *Engineering Fracture Mechanics*, 73(12):1711–1731, 2006.

[42] J. R. Yeh and I. G. Tadjbakhsh. Stress Singularity in Composite Laminates by Finite Element Method. *Journal of Composite Materials*, 20(4):347–364, 1986.

[43] N. Zhang and P. F. Joseph. A nonlinear finite elment eigenanalysis of singular stress fields in bimaterial wedges for plane strain. *International Journal of Fracture*, 94(4):299–319, 1998.

[44] O. C. Zienkiewicz and R. L. Taylor. *The finite element method for solid and structural mechanics*. Butterworth-Heinemann, 2005.